

Deep Unrestricted Document Image Rectification

Hao Feng[†], Shaokai Liu[†], Jiajun Deng, Wengang Zhou*, Senior Member, IEEE, and Houqiang Li*, Fellow, IEEE

Abstract—In recent years, tremendous efforts have been made on document image rectification, but existing advanced algorithms are limited to processing restricted document images, *i.e.*, the input images must incorporate a complete document. Once the captured image merely involves a local text region, its rectification quality is degraded and unsatisfactory. Our previously proposed DocTr, a transformer-assisted network for document image rectification, also suffers from this limitation. In this work, we present DocTr++, a novel unified framework for document image rectification, without any restrictions on the input distorted images. Our major technical improvements can be concluded in three aspects. Firstly, we upgrade the original architecture by adopting a hierarchical encoder-decoder structure for multi-scale representation extraction and parsing. Secondly, we reformulate the pixel-wise mapping relationship between the unrestricted distorted document images and the distortion-free counterparts. The obtained data is used to train our DocTr++ for unrestricted document image rectification. Thirdly, we contribute a real-world test set and metrics applicable for evaluating the rectification quality. To our best knowledge, this is the first learning-based method for the rectification of unrestricted document images. Extensive experiments are conducted, and the results demonstrate the effectiveness and superiority of our method. We hope our DocTr++ will serve as a strong baseline for generic document image rectification, prompting the further advancement and application of learning-based algorithms. The source code and the proposed dataset are publicly available at <https://github.com/fh2019ustc/DocTr-Plus>.

Index Terms—Document image rectification, Unrestricted document images, Transformer

I. INTRODUCTION

Nowadays, the widespread use of smartphones has led to a growing trend of directly using them for digitizing document files. Compared with traditional flatbed scanners, smartphones provide a more flexible, portable, and straightforward alternative for document image digitalization. However, those captured document images are inevitably distorted, due to some uncontrollable factors, including physical deformations of documents, illumination conditions, and camera angles. Such distortions block their digital storage and are likely to negatively impact downstream applications, such as automatic text recognition [1]–[4], analysis [5]–[7], retrieval [8]–[10], and question answering [11], [12]. Over the past few decades, document image rectification has been actively researched.

Hao Feng, Shaokai Liu, Wengang Zhou, and Houqiang Li are with the CAS Key Laboratory of Technology in Geo-spatial Information Processing and Application System, Department of Electronic Engineering and Information Science, University of Science and Technology of China, Hefei, 230027, China. Wengang Zhou, and Houqiang Li are also with Institute of Artificial Intelligence, Hefei Comprehensive National Science Center. E-mail: {haof, liushaokai}@mail.ustc.edu.cn; {zhwg, lihq}@ustc.edu.cn.

Jiajun Deng is with The University of Sydney, New South Wales, 2006, Australia. E-mail: jiajun.deng@sydney.edu.au.

[†]The first two authors contribute equal to this work.

*Corresponding authors: Wengang Zhou and Houqiang Li.

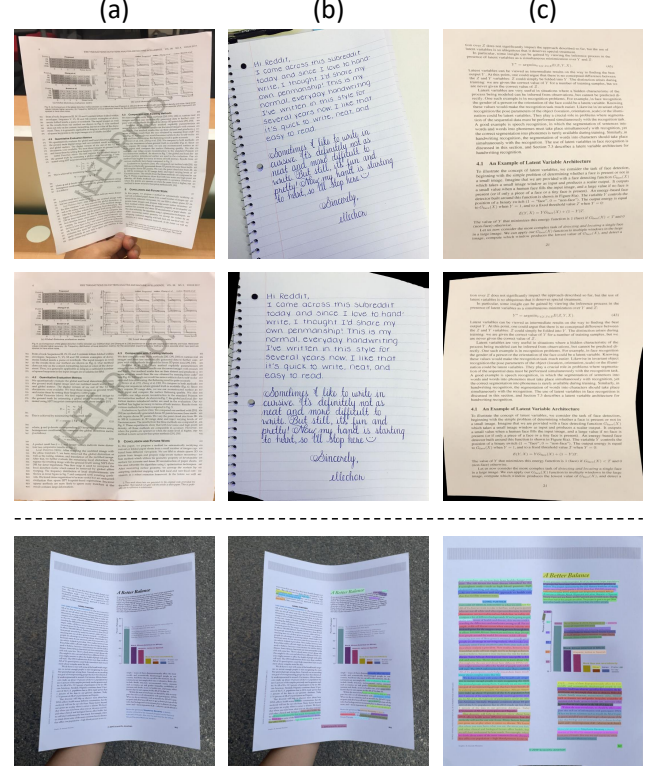


Fig. 1. Top row: three types of commonly distorted document images based on the presence of document boundaries: (a) w/ complete boundaries, (b) w/ partial boundaries, and (c) w/o any boundaries. Middle row: the rectified results of our method. Bottom row: the distorted image, the original detected texts, and the rectified one (highlighted), based on DBNet [31], [32].

In the literature, the conventional solutions are based on 3D reconstruction techniques. Generally, they construct a 3D representation of the captured distorted document and then flatten it into a distortion-free planar. To perform 3D reconstruction, some approaches resort to the auxiliary hardwares, such as structured-lighting system [13]–[15] or laser range scanner [16]. Other methods [17]–[21] capture multiview images of a document as an alternative. However, the extra hardwares and the demand for multiview images inevitably limit their usage in real applications. To overcome these limitations, some other methods assume a parametric model on the deformed surface of documents and optimize the model by extracting specific attributes, such as shading [22], [23], boundaries [24], textlines [25]–[29], or texture flow [30]. Nevertheless, the oversimplified parametric models usually lead to limited performance, and the optimization process introduces non-negligible computational cost.

Recently, deep learning based solutions [33]–[48] have been shown as an alternative to the traditional methods, with

promising performance and efficiency. By inferring a pixel-wise displacement field [49] from the distorted image to the distortion-free one with a deep network, a distorted document image can be unwarped with the predicted flow field at a high speed. However, most existing algorithms [33]–[47] are dedicated to processing restricted document images, *i.e.*, the input images must contain complete document boundaries (see Fig. 1(a)). Once the distorted images do not include complete document boundaries (see Fig. 1(b, c)), the rectification quality is degraded. To overcome this issue, DocProj [48] divides the input images into multiple patches and infers per-patch displacement field [49]. However, the stitching of the per-patch displacement field involves heavy computational cost [50] and this method is limited to rectifying the document images without any background regions (see Fig. 1(c)). For document images with some background regions, we need to manually cut out the document region first before the rectification. Therefore, a robust algorithm capable of rectifying various distorted document images in the wild is being sought.

As shown in Fig. 1, based on the existence of a complete document, a distorted document image can be divided into three categories, *i.e.*, (a) with complete boundaries, (b) with partial boundaries, and (c) with no boundaries. To adaptively rectify these cases with a unified model, in this study, we propose DocTr++, a novel deep network for unrestricted document image rectification. Our DocTr++ extends our previously proposed DocTr [36] that focuses on rectifying images containing complete documents, and makes improvements in the following three aspects. Firstly, we upgrade the architecture and adopt a hierarchical encoder-decoder structure for multi-scale representation learning and parsing, achieving improved distortion rectification. Secondly, to facilitate our motivation and train the network, we formulate the mapping relationship between the unrestricted distorted document images and the distortion-free counterparts. Thirdly, we contribute a real-world test set and metrics to evaluate the rectification quality in this scenario. To our best knowledge, this is the first learning-based method for rectifying unrestricted document images.

Extensive experiments are conducted on our proposed dataset and the challenging DocUNet Benchmark dataset [39]. The quantitative and qualitative results showcase the effectiveness and superiority of our method over existing solutions. We hope that our DocTr++ will serve as a strong baseline for unrestricted document image rectification, encouraging further advancement and application of learning-based algorithms for document image rectification.

In summary, we make three-fold contributions as follows:

- We make the first attempt to unrestricted document image rectification, and propose a novel solution, *i.e.*, DocTr++, adopting a hierarchical encoder-decoder structure for effective representation encoding and parsing.
- We contribute a new document image dataset and applicable metrics to facilitate the training and evaluation for unrestricted document image rectification.
- We conduct extensive experiments to validate the merits of our method and sets several new state-of-the-art records on the prevalent and proposed benchmarks.

II. RELATED WORK

In this section, we categorize the previous works on document image rectification into two groups: (a) rectification based on 3D reconstruction, and (b) rectification based on deep learning, discussed in the following.

A. Rectification Based on 3D Reconstruction

Traditional solutions for document image rectification rely on the 3D reconstruction techniques. These methods [13]–[16] commonly first reconstruct the 3D shape of a deformed document page and then flatten it to a planar shape. Typically, Brown and Seales [14] first employed a structured light 3D acquisition system for 3D model reconstruction. Zhang et al. [16] adopted a laser range scanner instead and performed restoration based on a physical modeling technique. Meng et al. [15] utilized two structured beams to illuminate upon the deformed document page and obtained its developable surface for rectification. While these methods have shown effectiveness in real-world scenarios, they require additional hardware to scan the deformed documents, making them less practical for personal use.

Some methods work from multiview images of a document for 3D reconstruction. Typically, Tsoi et al. [19] convert the multiview images to a canonical coordinate frame based on the document boundary interpolation [20]. Koo et al. [17] match the corresponding points in two views by SIFT [51] to estimate document surface model. Based on the ridge-aware 3D reconstruction techniques, You et al. [21] propose a general developable surface models that can represent a wide variety of paper deformations. For such above works, the complicated image acquisition steps still limit their further applications.

To address the above issues, other methods reconstruct the 3D model from a single-view image. They first assume a parametric model on the document surface and then fit the model by extracting the specific representations, including shading [22], [23], boundaries [24], textlines [25]–[29], or texture flow [30]. Typically, using a proximal light source, Wada et al. [23] recover the 3D shape of an unfolded book surface based on the shading distribution. He et al. [24] extract a book boundary model for the reconstruction of 3D book surface. Textline-based method [25]–[28] segment the textlines in distorted document pages to estimate the parameters of the surface model. Besides, Meng et al. [52] recover the 3D page shape by exploiting the intrinsic vector fields of the image. However, these methods still have some limitations. On the one hand, the fixed parametric models are not usually applicable to the complicated real geometric distortions of deformed documents. On the other hand, the optimization process introduces non-negligible computational cost.

B. Rectification Based on Deep Learning

Deep learning has been introduced recently and shown as a promising alternative to the conventional works. By predicting a pixel-wise displacement field [49] with a deep network, a distorted document image can be rectified by resampling the pixels from the input distorted image to the rectified one.

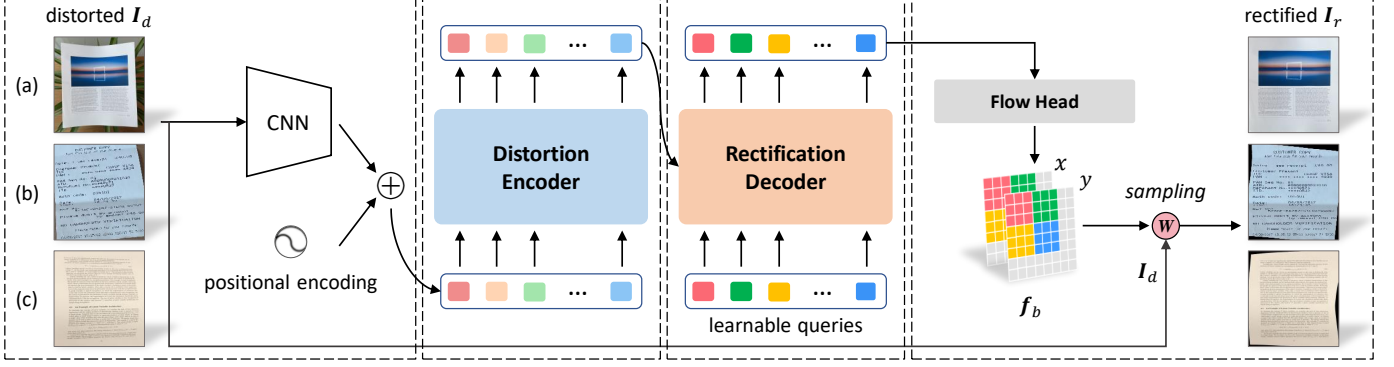


Fig. 2. An overview of our DocTr++ for unrestricted document image rectification. Given an arbitrary distorted document image I_d , we extract its features through a CNN backbone and a distortion encoder architecture. Then, the rectification decoder takes a fixed number of learned queries as input that attend to the encoder’s output. These embeddings are parallelly transformed into per-patch warping flows f_b pointing to I_d . Finally, we use the predicted f_b to warp I_d and obtain the rectified image I_r through the bilinear sampling-based warping operation “W”.

As a pioneering work, DocUNet [39] regresses a pixel-wise displacement field with a stacked UNet [53] to un warp the input distorted document image. DocProj [48] divides the input distorted document image into multiple patches, estimates the per-patch displacement field, and finally stitches them for full image rectification. Using a fully convolutional network [54], Xie et al. [41] supplement an explicit regularization to control the smoothness of the displacement field. Inspired by the traditional methods based on 3D reconstruction, Amir et al. [45] and Das et al. [34] model the 3D shape of a deformed document in the network. DocTr [36] introduces transformer [55] from natural language processing tasks to improve the representation learning of document images.

Different from the pixel-wise flow regression, DDCP [40] only estimates several control points and reference points to perform rectification, based on the TPS interpolation algorithm [56]. PWUNet [35] considers the different distortion degrees of local patches and estimate local deformation fields for improved global unwarping. DocGeoNet [44] proposes to encode representations of rectification cues to improve rectification, by detecting textlines in the network. RDGR [37] first detect textlines and document boundaries, and then obtain the rectified image by solving an optimization problem based on the proposed grid regularization. FDRNet [42] concentrates on high-frequency components in the Fourier space to capture structural information of deformed documents for improved rectification. Marior [47] considers the document images with large marginal regions and gradually rectifies them to a robust state. DocScanner [43] proposes to rectify the distortion in a progressive and iterative manner with a lightweight network. PaperEdge [46] boosts document unwarping performance by introducing real-world document images in the training. CGU-Net [57] introduces a novel grid-based method for document unwarping and contributes a high-quality synthetic dataset.

Although the above learning-based works are reported with state-of-the-art performance and running efficiency, they are still limited to processing document images with a controlled appearance. Among them, methods [34]–[48] can only process images with complete document and the captured documents are surrounded by a limited size background area. Besides,

Marior [47] innovatively proposes to rectify the images with larger background areas, while DocProj [48] mainly considers the samples with no background regions. In contrast, in this work, we aim to achieve an adaptive rectification of various document images in the wild, regardless of whether or not they incorporate complete document boundaries. We hope that our method will provide a strong baseline and attract new researchers to the field, prompting the real applications of document image rectification algorithms.

III. APPROACH

Fig. 2 shows an overview of our DocTr++. Given a distorted document image I_d , we first utilize a conventional CNN backbone [58] to extract its 2D representation and feed it to a distortion encoder [55]. Then, a rectification decoder [55] takes as input a fixed number of learned embeddings that attends to the output of the encoder, and decodes per-patch warping flow f_b pointing at pixels in distorted image I_d . With the predicted f_b , we sample the pixels from image I_d to reconstruct the rectified image I_r . Different from previous methods, for our DocTr++, the input document images I_d cover various situations captured in daily life, including (a) with complete document boundaries, (b) with partial document boundaries, and (c) without any document boundaries. In the following, we separately discuss the four main components of our DocTr++, including (a) backbone, (b) distortion encoder, (c) rectification decoder, and (d) flow head.

A. Backbone

Starting from an arbitrary distorted document image $I_d \in \mathbb{R}^{H \times W \times 3}$, where H and W denote the height and width of this RGB image, we first extract its features with a convolutional module. This convolutional module consists of 6 residual blocks [58]. It downsamples the feature maps at $\frac{1}{2}$ resolution every two residual blocks and finally produce feature map $E_c \in \mathbb{R}^{\frac{H}{8} \times \frac{W}{8} \times C_b}$, where we set $C_b = 256$.

B. Distortion Encoder

To rectify a distorted document image, it is essential to capture its structural information. However, in a document image, such information usually exists in components distributed

among non-local regions, such as curved textlines and textures with gradually changing light appearance. To encode the structural information for an improved rectification, we propose to introduce the self-attention mechanism from transformer [55] and construct a hierarchical distortion encoder.

Specifically, as shown in Fig. 3, the distortion encoder consists of three blocks and each block contains two standard transformer encoder layers [55]. To generate both high-resolution fine features and low-resolution semantically stronger features, we downsample the feature maps at $\frac{1}{2}$ resolution with a convolutional layer ($stride = 2$) after the first and second blocks. Since the transformer architecture [55] is permutation-invariant, we supplement the image features with the fixed 2D position embedding \mathbf{P}_e [59] before the transformer encoder layer. Each layer contains a multi-head self-attention module and a feed-forward network. The output representation in each layer can be calculated as follows,

$$\mathbf{E}_0 = \mathbf{E}_c + \mathbf{P}_e,$$

$$\mathbf{E}'_i = LN(MA(\mathbf{E}_{i-1}, \mathbf{E}_{i-1}) + \mathbf{E}_{i-1}), i = \{1, \dots, 6\}, \quad (1)$$

$$\mathbf{E}_i = LN(FFN(\mathbf{E}'_i) + \mathbf{E}'_i), i = \{1, \dots, 6\},$$

where $MA(\cdot)$, $FFN(\cdot)$, and $LN(\cdot)$ are the multi-head attention, feed-forward network, and layer normalization, respectively, \mathbf{E}_i denotes the output feature of the i^{th} encoder layer.

C. Rectification Decoder

As shown in Fig. 3, the rectification decoder takes as input the hierarchical feature maps $\{\mathbf{E}_2, \mathbf{E}_4, \mathbf{E}_6\}$ from the distortion encoder as well as a small fixed number of learned embeddings $\mathbf{D}_l \in \mathbb{R}^{(\frac{H}{8} \times \frac{W}{8}) \times C_b}$. It outputs the features for predicting the warping flow $\mathbf{f}_b \in \mathbb{R}^{H \times W \times 2}$ used to rectify the input distorted image \mathbf{I}_d . We term the learned embeddings as the rectification queries and each query is responsible for the rectification of a corresponding region in the input distorted image.

The rectification decoder consists of three blocks and each block includes two standard transformer decoder layers [55]. For the first block, we take as input the learnable embedding $\mathbf{D}_l \in \mathbb{R}^{\frac{H}{32} \times \frac{W}{32} \times C_b}$ to attend to the feature map $\mathbf{E}_6 \in \mathbb{R}^{\frac{H}{32} \times \frac{W}{32} \times C_b}$. For the other two blocks, we take the currently decoded embeddings as input to attend to the feature map $\mathbf{E}_4 \in \mathbb{R}^{\frac{H}{16} \times \frac{W}{16} \times C_b}$ and $\mathbf{E}_2 \in \mathbb{R}^{\frac{H}{8} \times \frac{W}{8} \times C_b}$, respectively. Note that the decoded embeddings of the first and second blocks are upsampled based on the bilinear interpolation when fed into the next block. Each decoder layer consists of a multi-head self-attention module, an encoder-decoder multi-head attention module, and a feed-forward network. The formula in each layer is given as follows,

$$\mathbf{D}_0 = \mathbf{D}_l + \mathbf{P}_d,$$

$$\mathbf{D}'_i = LN(MA(\mathbf{D}_{i-1}, \mathbf{D}_{i-1}) + \mathbf{D}_{i-1}), i = \{1, \dots, 6\},$$

$$\mathbf{D}''_i = LN(MA(\mathbf{D}'_i, \mathbf{E}_k) + \mathbf{D}'_i), i = \{1, \dots, 6\}, k = \{2, 4, 6\},$$

$$\mathbf{D}_i = LN(FFN(\mathbf{D}''_i) + \mathbf{D}''_i), \quad (2)$$

where \mathbf{D}_i indicates the output of the i^{th} decoder layer, \mathbf{P}_d represents the positional embeddings [59], and \mathbf{E}_k denotes the attended features from the corresponding encoder block.

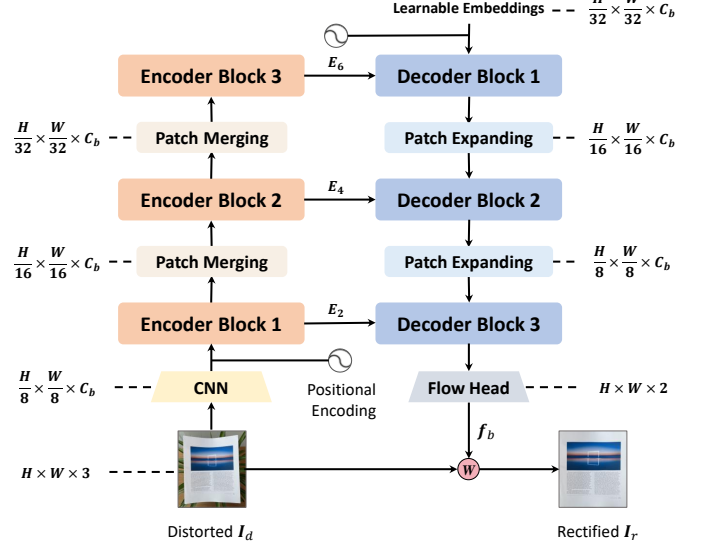


Fig. 3. Detailed architecture of the proposed DocTr++. It takes a hierarchical architecture that incorporates a distortion encoder for multi-level feature extraction and a rectification decoder for warping flow prediction.

D. Flow Head

Given the decoded features $\mathbf{D}_6 \in \mathbb{R}^{\frac{H}{8} \times \frac{W}{8} \times C_b}$, we introduce a learnable upsampling module [36] to predict the warping flow $\mathbf{f}_b \in \mathbb{R}^{H \times W \times 2}$ for rectifying the distorted image \mathbf{I}_d .

Specifically, we first apply two convolutional layers to the feature map $\mathbf{D}_6 \in \mathbb{R}^{\frac{H}{8} \times \frac{W}{8} \times C_b}$ and produce the coarse warping flow $\mathbf{f}_m \in \mathbb{R}^{\frac{H}{8} \times \frac{W}{8} \times 2}$. Then, we exploit another two convolutional layers to process $\mathbf{D}_6 \in \mathbb{R}^{\frac{H}{8} \times \frac{W}{8} \times C_b}$, and reshape the output feature map to shape $\frac{H}{8} \times \frac{W}{8} \times 8 \times 8 \times 9$. Next, we perform softmax on the last dimension of it and get the weight matrix. Using the obtained weight matrix, we take a weighted combination over the 3×3 neighborhood of each pixel in \mathbf{f}_m . Finally, the obtained $\frac{H}{8} \times \frac{W}{8} \times 8 \times 8 \times 2$ map is permuted and reshaped to the full resolution warping flow map $\mathbf{f}_b \in \mathbb{R}^{H \times W \times 2}$. With the predicted \mathbf{f}_b , the rectified document image $\mathbf{I}_r \in \mathbb{R}^{H \times W \times 3}$ can be obtained by a warping operation based on the bilinear interpolation as follows,

$$\mathbf{I}_r(u_0, v_0) = \mathbf{I}_d(\mathbf{f}_b^u(u_0, v_0), \mathbf{f}_b^v(u_0, v_0)), \quad (3)$$

where $\mathbf{f}_b^u \in \mathbb{R}^{H \times W \times 1}$ and $\mathbf{f}_b^v \in \mathbb{R}^{H \times W \times 1}$ are the horizontal and vertical coordinate mapping matrix in \mathbf{f}_b , respectively, and (u_0, v_0) is the pixel coordinate.

During training, the loss function is defined as the L_1 distance between the predicted warping flow \mathbf{f}_b and its given ground truth \mathbf{f}_{gt} as follows,

$$\mathcal{L} = \|\mathbf{f}_{gt} - \mathbf{f}_b\|_1. \quad (4)$$

IV. DATASET AND METRICS

To facilitate training and evaluation of the algorithms for unrestricted document image rectification, we first present the UDIR, a new dataset for unrestricted document image rectification. Furthermore, we contribute the new quantitative metrics applicable for evaluating the rectification quality in terms of image similarity and distortion rectification. In the following, we elaborate them separately.

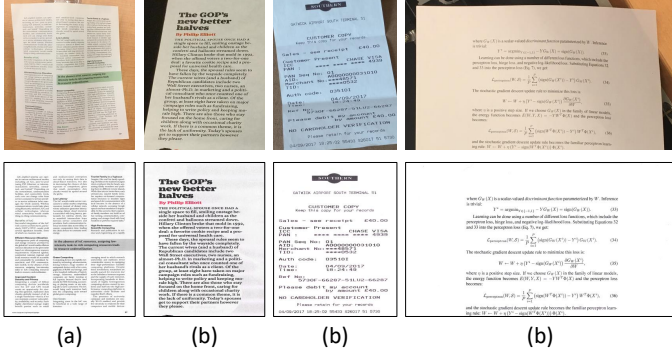


Fig. 4. Sample images in the UDIR test set. The first and second rows show the distorted and ground truth images, respectively. (a), (b), and (c) represent the images with complete document boundaries, with partial document boundaries, and without any document boundaries, respectively.

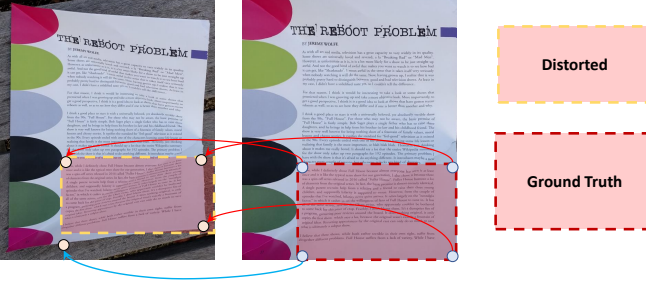


Fig. 5. Illustration of the mapping relationship between the distorted image (with no boundaries) and the distortion-free one. The distortion-free image should cover the all content of the distorted one. Therefore, there are unexpected redundant regions that do not exist in the distorted one, highlighted with the blue arrow. The obtained warping flow is continuously distributed.

A. UDIR Dataset

Training Set. The training set is extended from the classic Doc3D dataset [34]. It contains 100k distorted document images and their distortion-free ground truth. In Doc3D [34], each distorted image contains a complete document surrounded by a background region. To construct the training set for unrestricted document image rectification, we randomly crop such distorted document images to meet one of the following three conditions, including (a) with complete document boundaries, (b) with partial document boundaries, and (c) without any document boundaries, as illustrated in Fig. 2.

Meanwhile, to compose the backward warping flow as the ground truth for distortion rectification, we formulate the pixel-wise mapping relationship between each obtained distorted image and the corresponding distortion-free one, as illustrated in Fig. 5. Note that the distortion-free image should cover the all content of the distorted one. Therefore, there are unexpected redundant regions that do not exist in the distorted one (blue arrow in Fig. 5). The obtained flow is continuously distributed, but this does not affect its learning. During the inference stage, the predicted flow pointing outside the input image directly fetches a fixed pixel value. We set them as zero by default, which makes up the black regions in the rectified image (see the rectified images of DocTr++ in Fig. 8).

Test Set. Considering that there is no benchmark dataset for the evaluation of unrestricted document image rectification,

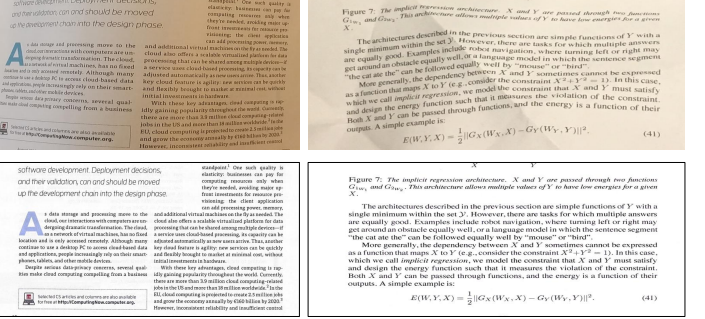


Figure 7: The implicit regression architecture. X and Y are passed through two functions $G_{X(w)}$ and $G_{Y(w)}$. This architecture allows multiple values of Y to have low energies for a given X .

The architectures described in the previous section are simple functions of Y with a single minimum with the set \mathcal{Y} . However, in some cases, the functions can be equal to zero. Examples include robot navigation, where turning left or right may get around an obstacle equally well, or a language model in which the sentence segment “the cat and the dog” is followed equally well by “meow” or “bark”.

More generally, the dependency between X and Y sometimes cannot be expressed as a function that maps X to Y . In this case, we call Y sometimes called a latent variable, and we call $G_X(w)$ and $G_Y(w)$ the encoder and decoder of the constraint. Both X and Y can be passed through functions, and the energy is a function of their outputs. A simple example is

$$E(W, Y, X) = \frac{1}{2} ||G_X(W_X, X) - G_Y(W_Y, Y)||^2. \quad (41)$$

we further construct a dataset that contains real-world camera-captured document images. The dataset is extended from the classic DocUNet Benchmark dataset [39] that consists of 130 real document images and their ground truth. Similarly, we manually crop such images to meet one of the following three conditions, including (a) with complete document boundaries, (b) with partial document boundaries, and (c) without any document boundaries. The test set contains 195 images in total, and each of the three situations accounts for one-third. Fig. 4 presents some examples of our UDIR test set. We can see that the proposed test set covers the common distorted document images captured in daily life.

B. Metrics

Fig. 7(a) illustrates the evaluation way of typical metrics MSSIM, ED, CER, and LD, where the input distorted image should contain a complete document. As shown in Fig. 7(b), when the situation comes to the unrestricted document images, these metrics are no longer applicable, due to the unexpected black regions in rectified images. Hence, we further propose metrics MSSIM-M and LD-M, described next.

MSSIM-M. Structural SIMilarity (SSIM) [60] measures the per-patch similarity between two images. Since the perceptibility of details rely on the sampling density of the image, Multi-scale Structural Similarity (MSSIM) [61] calculates the weighted summation of SSIM [60] across multiple scales. For document image rectification, all the rectified and ground truth flatbed-scanned images are first resized to a 598,400-pixel area, as recommended in DocUNet [39]. Then, it is computed with a 5-level-pyramid, following original MSSIM [61]. However, when the input distorted images do not contain complete documents, there will be some black regions in the rectified images, inconsistent with the ground truth one (see Fig. 4). To address the issue, we first mask the manually cropped ground truth image with these black regions and then calculate the MSSIM (see Fig. 7(b)). We term the obtained score as Multi-scale SIMilarity Masked (MSSIM-M).

LD-M. Local distortion (LD) [21] first match the rectified image with the ground truth one using a dense SIFT-flow [62] $(\Delta x, \Delta y)$, where Δx and Δy denote the horizontal and vertical displacement map of the matched pixels from the ground truth image to the rectified one, respectively. LD is defined

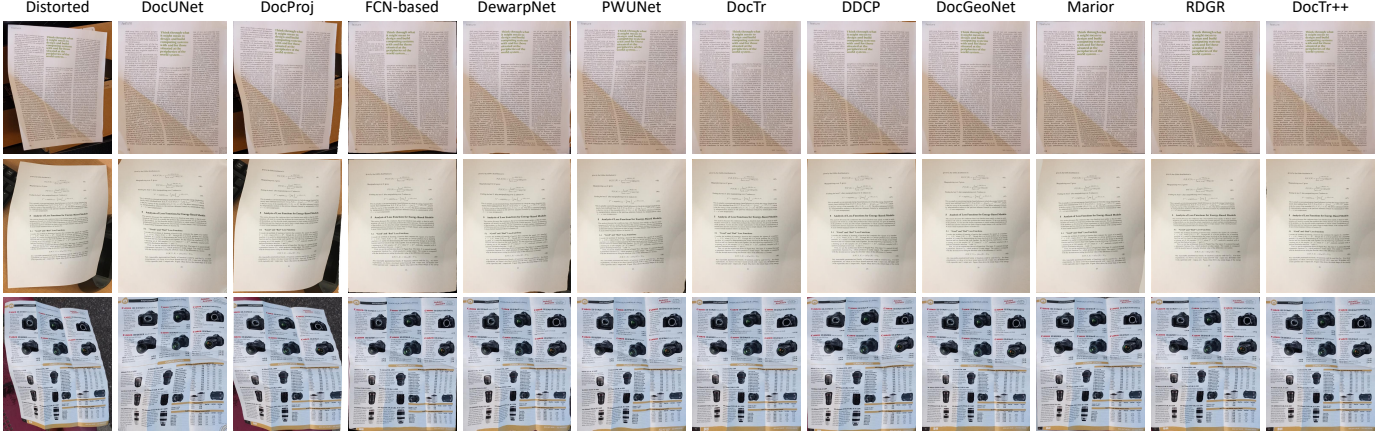


Fig. 6. Qualitative comparisons with existing learning-based methods, including DocUNet [39], DocProj [48], FCN-based [41], DewarpNet [34], PWUNet [35], DocTr [36], DDCP [40], DocGeoNet [44], Marior [47], RDGR [37], and our DocTr++, from left to right.

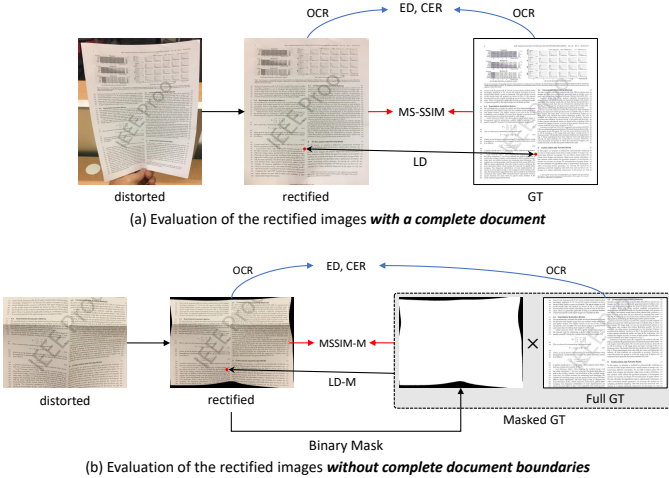


Fig. 7. Illustration of the different ways for evaluating the rectified images (a) including a complete document and (b) without complete document boundaries. For the latter, to calculate the proposed MSSIM-M and LD-M, the original full GT image is first masked by the black regions in the rectified image. “ \times ” denotes pixel-wise multiplication.

as the mean L_2 distance among all matched pixels, which measures the average local deformation of the rectified image. Then, our Local Distortion Masked (LD-M) is calculated as the mean L_2 distance in the valid regions of the rectified image, avoiding the invalid matches in the black regions.

ED and CER. Edit Distance (ED) [63] measures how dissimilar two strings are to one another, which is defined as the minimum number of operations required to transform one string into the reference one. It can be efficiently computed based on the dynamic programming algorithm. Specifically, the involved operations include deletions (d), insertions (i), and substitutions (s). Then, Character Error Rate (CER) can be computed as follows,

$$CER = (d + i + s)/N_c, \quad (5)$$

where N_c is the character number of the reference string. CER depicts the percentage of characters in the reference text incorrectly recognized in the rectified image. The lower

TABLE I
QUANTITATIVE COMPARISONS WITH EXISTING METHODS ON THE DOCUNET BENCHMARK DATASET [39]. “ \uparrow ” INDICATES THE HIGHER THE BETTER AND “ \downarrow ” MEANS THE OPPOSITE.

Methods	Venue	MSSIM \uparrow	LD \downarrow	ED \downarrow	CER \downarrow
Distorted	/	0.25	20.51	1552.22	0.5089
DocUNet [39]	CVPR'18	0.41	14.19	1259.83	0.3966
DocProj [48]	TOG'19	0.29	18.01	1165.93	0.3818
FCN-based [41]	DAS'20	0.45	7.84	1031.40	0.3156
DewarpNet [34]	ICCV'19	0.47	8.39	525.45	0.2102
DocTr [36]	MM'21	0.51	7.76	464.83	0.1746
PWUNet [35]	ICCV'21	0.49	8.64	743.32	0.2623
DDCP [40]	ICDAR'21	0.47	8.99	745.35	0.2626
DocGeoNet [44]	ECCV'22	0.50	7.71	379.00	0.1509
Marior [47]	MM'22	0.48	7.44	593.80	0.2136
RDGR [37]	CVPR'22	0.50	8.51	420.25	0.1559
DocTr++	/	0.51	7.52	447.47	0.1695

the CER value (with 0 being a perfect score), the better the performance of the rectification method. As shown in Fig. 7, since N_c is a constant for the full GT image, here we do not mask it with the rectified black regions, which does not affect the evaluation of OCR performance.

V. EXPERIMENTS

A. Implementation Detail

Inference Way. Following DocTr [36], during training, the image size (H, W) is set as (288, 288). For evaluation, the real-world distorted document images of arbitrary resolutions are first resized to (288, 288). The obtained images are then fed into the network that produces a warping flow of shape (288, 288). Finally, we resize the flow map to the original shape of the input distorted image and unwarped it with the obtained flow map. In this way, we produce the output high-resolution rectified document image with legible text.

Training. We use the AdamW optimizer [64] and OneCycle learning rate schedule [65] with a maximum learning rate of 10^{-4} . The epochs for the warm-up phase account for 10%. The network is trained for 65 epochs with a batch size of 12. We employ 4 NVIDIA GeForce RTX 2080Ti GPUs for

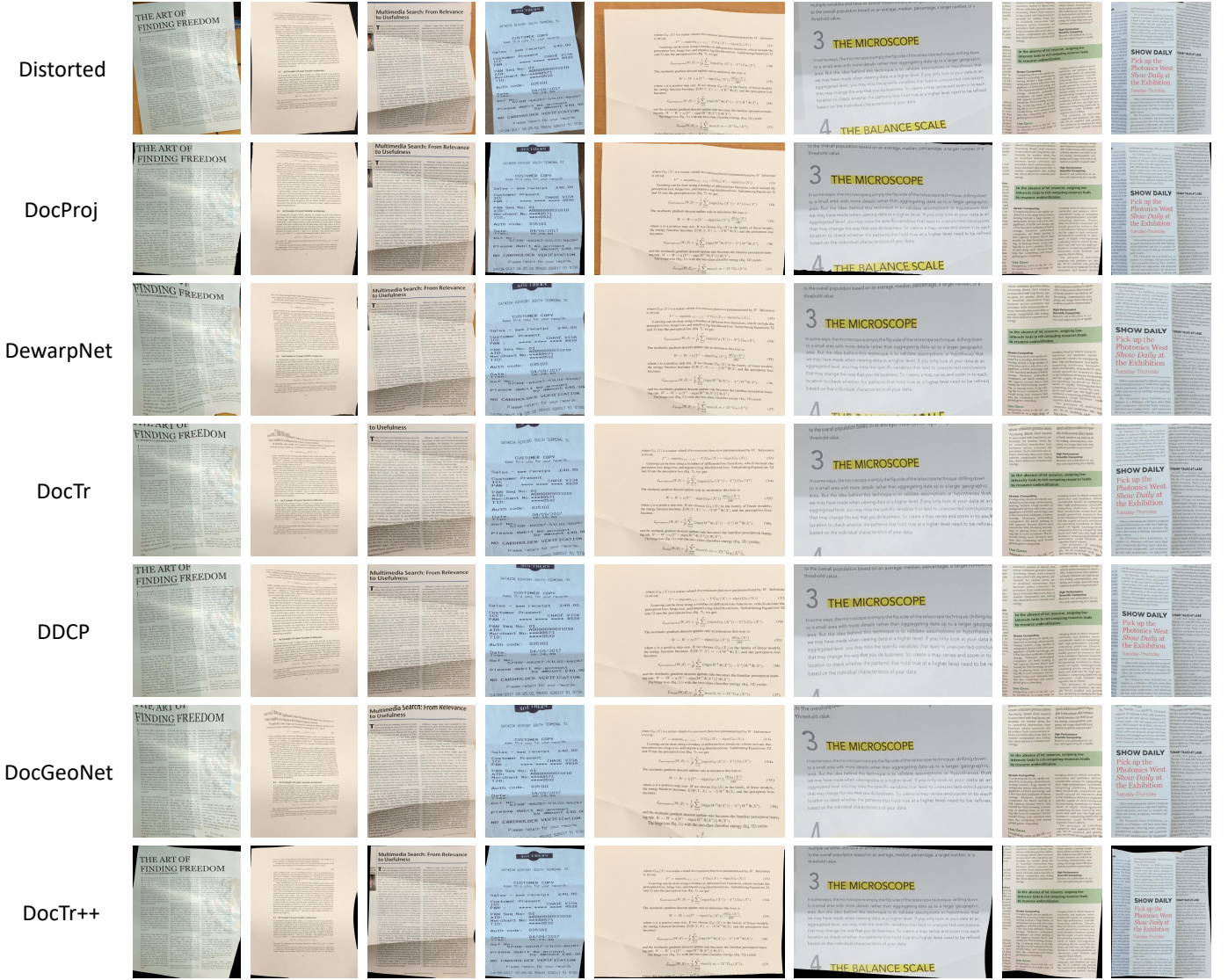


Fig. 8. Qualitative results of DocTr++ and other methods on the UDIR test set. The first row shows the input distorted document images, and the other rows are rectified results of the corresponding methods. The results of our DocTr++ present less distortion than the other methods.

TABLE II
QUANTITATIVE COMPARISONS WITH EXISTING METHODS ON THE PROPOSED UDIR TEST SET. “ \uparrow ” INDICATES THE HIGHER THE BETTER AND “ \downarrow ” MEANS THE OPPOSITE.

Methods	Venue	MSSIM-M \uparrow	LD-M \downarrow	ED \downarrow	CER \downarrow
Distorted	/	0.31	18.87	1181.47	0.3986
DocProj [48]	TOG’19	0.31	19.11	932.11	0.2995
DewarpNet [34]	ICCV’19	0.36	17.91	1037.04	0.3454
DocTr [36]	MM’21	0.38	18.80	840.67	0.2988
DDCP [40]	ICDAR’21	0.36	19.26	984.63	0.3324
DocGeoNet [44]	ECCV’22	0.38	18.60	872.69	0.3024
DocTr++	/	0.45	12.47	666.49	0.2288

training. Besides, to generalize better to real data with complex illumination conditions, we add a jitter in the HSV color space to magnify illumination and document color variations.

Evaluation. Firstly, to calculate MSSIM and MSSIM-M,

the weight for each level of the image pyramid is set as 0.0448, 0.2856, 0.3001, 0.2363, and 0.1333, following methods [36], [43], [44]. The Matlab version is 2019a. Secondly, we use Tesseract (v5.0.1) [66] as the OCR engine to recognize the text string of the rectified image and the ground truth one, as recommended in previous works [36], [43], [44]. For the DocUNet Benchmark dataset [39], we select 60 images for OCR evaluation, following DocTr [36]. For our UDIR test set, we select 70 images. In such selected images, the text should make up the majority of the content. This reason is that if the text is rare in an image, the character number N_c (numerator) in Equation (5) is a small number, which would lead to a significant variance for CER.

Notably, we observe that the 127th and 128th distorted document images in the DocUNet Benchmark dataset [39] are rotated by 180 degrees, which do not match the ground truth documents. This inconsistency is ignored by our DocTr [36] and many previously published methods [34]–[42], [45]–[48].

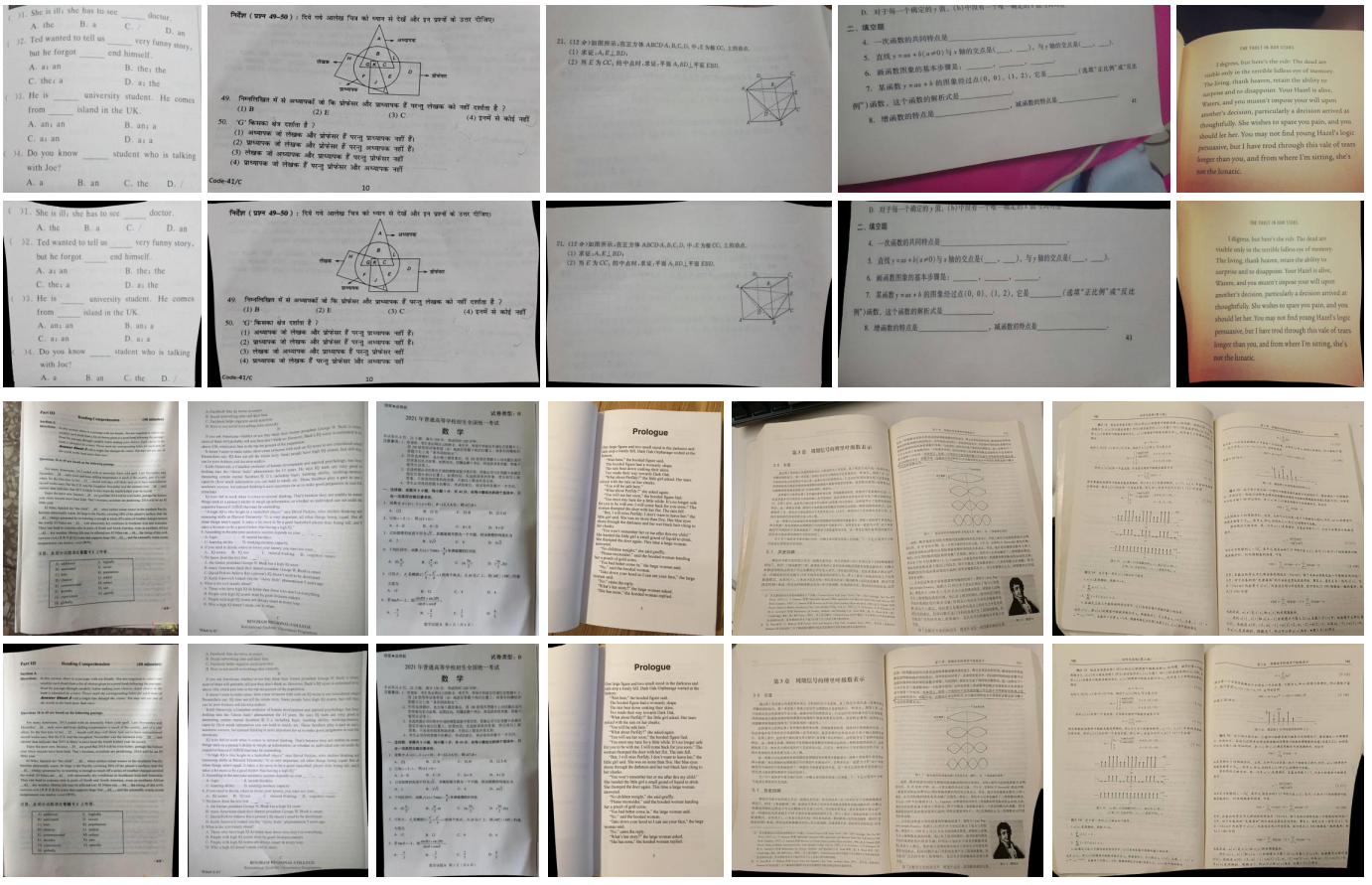


Fig. 9. Qualitative results of DocTr++ on some common real-world distorted document images, including test papers, book pages, and text paragraphs. The first and third rows display the input distorted images, while the second and fourth rows present their corresponding rectified results.

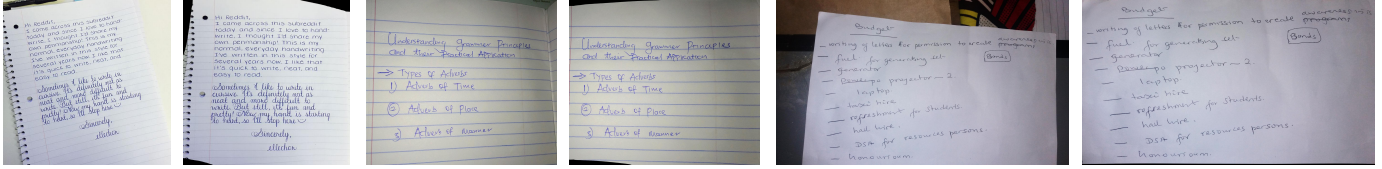


Fig. 10. Qualitative results of DocTr++ on three real-world distorted handwriting images. For each sample, we show the distorted and rectified images, from left to right. Such distorted document images do not contain complete document boundaries. They are effectively restored and the rectified textlines are straight along the horizontal direction.

In this paper, the reported performances of our DocTr++ and other methods are based on the corrected dataset.

B. Experimental Results

We quantitatively and qualitatively evaluate the proposed DocTr++ with existing learning-based methods. The evaluation is conducted on the widely-used DocUNet Benchmark dataset [39] and the proposed UDIR test set. Note that different from the former dataset, the latter one contains various images with complete or incomplete document boundaries.

Quantitative Comparison. We first compare DocTr++ with the existing learning-based methods on the DocUNet Benchmark dataset [39]. As mentioned above, all the distorted images in this dataset incorporate complete documents. Following prior methods [36], [41], [43], [44], [47], we add

a document localization module to remove the noisy backgrounds around the document before the distortion rectification. Here we adopt the same pre-possessing module [67] used in DocTr [36]. The comparison results are shown in Table I. Compared with DocTr [36], DocTr++ improves LD and CER from 7.76 to 7.52 and 17.46% to 16.95%, respectively. Moreover, our DocTr++ also shows comparable performance with the state-of-the-art RDGR [37] and outperforms the recent Marior [47] on metric CER by 4.41%.

Table II summarizes the results of our DocTr++ and the previously published methods on the proposed UDIR test set. Note that here we only compare the methods with released codes. As we can see, our DocTr++ performs better than these methods on all metrics. Notably, we outperform DocTr on MSSIM-M by 7% and yield an improvement on LD-M by 33.67%. Such results indicate the restoration ability of

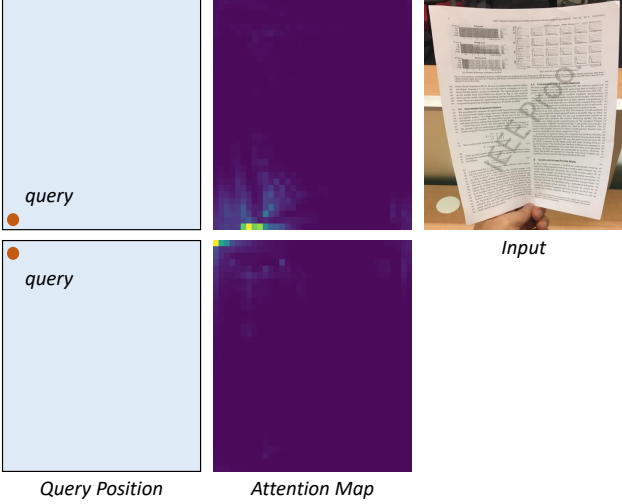


Fig. 11. Attention map visualization of the learnable query in the rectification decoder. We take the attention maps from its last block. As we can see, each query is responsible for the rectification of a specific region in the input distorted image that is accurately attended. The visualization effectively illustrates the role of the learnable queries in our method.

TABLE III
QUANTITATIVE COMPARISONS BETWEEN DOCTR [36] AND DOCTR++ ON THE COMPUTATIONAL COMPLEXITY AND PARAMETER COUNTS. “ \uparrow ” INDICATES THE HIGHER THE BETTER AND “ \downarrow ” MEANS THE OPPOSITE.

Methods	Venue	#Flops \downarrow	#Params \downarrow
DocTr [36]	MM’21	53G	25.7M
DocTr++	/	34G	26.6M

DocTr++ on processing unrestricted document images.

Qualitative Comparison. To clearly show the effectiveness of our DocTr++, we carry out qualitative comparisons with other existing methods to provide visual evidence.

Firstly, in Fig. 6, we qualitatively compare the rectified results of DocTr++ and the existing learning-based methods on the DocUNet Benchmark dataset [39]. As we can see, our DocTr++ reveals superior rectification performance. Secondly, as shown in Fig. 8, we present the rectified results of DocTr++ and other learning-based methods on the proposed UDIR test set. As can be seen, our method can effectively rectify the unrestricted distorted document images including incomplete documents or local text paragraphs. Compared with previous methods, our rectified images reveal less distortion. These results demonstrate the strong generation ability of our method in restoring various real-world distorted document images.

Efficiency Comparison. In addition to achieving better rectification performance than DocTr [36], we also compare their computational complexity and parameter counts. The results are shown in Table III. Compared with DocTr [36], our DocTr++ has slightly more parameters, but a much lower computational complexity, thanks to its hierarchical architecture that effectively reduces the $O(N^2)$ complexity of the self-attention process [55].

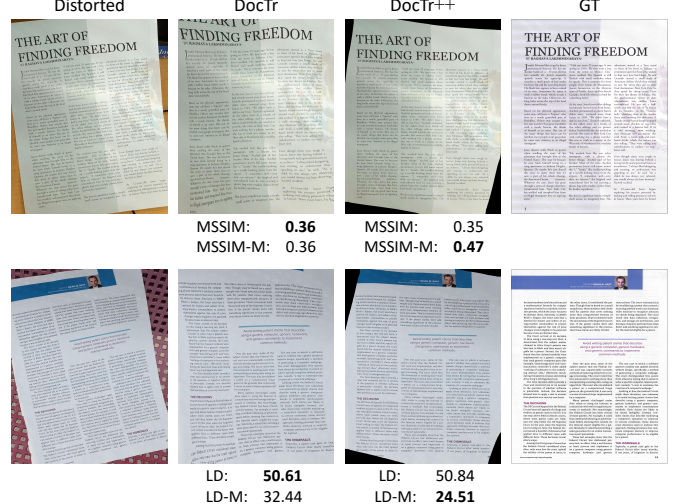


Fig. 12. Failure cases of metric MSSIM and LD. Compared with DocTr [36], the rectified images of DocTr++ show less distortion. However, the metric MSSIM and LD can not well perceive their difference, while the proposed MSSIM-M and LD-M are more robust and reliable.

TABLE IV
ABLATIONS ABOUT THE NETWORK ARCHITECTURE OF DOCTR++ ON THE PROPOSED UDIR TEST SET. “ \uparrow ” INDICATES THE HIGHER THE BETTER AND “ \downarrow ” MEANS THE OPPOSITE. SETTINGS USED IN OUR FINAL MODEL ARE UNDERLINED.

Methods	Setting	MSSIM-M \uparrow	LD-M \downarrow	ED \downarrow	CER \downarrow
Encoder	<u>w/</u> w/o	0.45	12.47	666.49	0.2288
	0.44	12.47	680.44	0.2353	
Decoder	<u>w/</u> w/o	0.45	12.47	666.49	0.2288
	0.45	12.56	684.67	0.2293	
Query	<u>learned</u> fixed	0.45	12.47	666.49	0.2288
	0.45	12.52	717.81	0.2408	
Upsample	<u>learned</u> bilinear	0.45	12.47	666.49	0.2288
	0.45	12.77	689.97	0.2375	
Flow	<u>continuous</u> discontinuous	0.45	12.47	666.49	0.2288
	0.44	12.96	715.43	0.2421	

C. Ablation Study

We further conduct extensive quantitative and qualitative experiments to validate each component of our DocTr++.

Architecture Setting. Table IV studies the architecture setting of DocTr++. Without either the distortion encoder or the rectification decoder, the performances become worse. It should be noted that in the both experiments, the number of the transformer encoder or decoder layer is set as 12, equal to our DocTr++. The results demonstrate the significance of a strong encoder and decoder for distortion representation learning and distortion correction prediction, respectively. Then, we study the learnable query with a fixed one. As we can see, performances are better with the learnable query. Next, we validate the upsample module [36] for warping flow prediction. We can see that, compared with the bilinear upsample module, the learnable one produces better performance. The likely reason is that the learnable way is capable of rectifying finer deformations. As mentioned in Sec. IV-A, our ground truth warping flow is continuously distributed. To ablate it, we

set the flow that points to the outside of the input distorted image as value -1 , following DocUNet [39]. The results show that learning the continuously distributed flow map is more effective and yields better performance.

To better illustrate the role of the query that is the input to the rectification decoder, we visualize the attention map of some typical queries. As shown in Fig. 11, each query is responsible for rectifying a specific region in the input distorted image that is accurately attended. Such explainable results explain how our decoder works. This mechanism is similar to the classic detector DETR [68], where the object queries are used to decode the boxes with specific patterns.

Robustness of Proposed Metrics. In Fig. 12, we show two failure cases of the metric MSSIM and LD in evaluating the rectified unrestricted document images. As we can see, compared with DocTr [36], the rectified images of DocTr++ are less distorted. Nevertheless, MSSIM and LD cannot effectively reveal their difference, due to the black area existing in the rectified image. In contrast, the proposed MSSIM-M and LD-M are more robust and reliable.

Other Results. To better evaluate our method, we collect some other real-world distorted document images, including test papers, book pages, and text paragraphs. The rectified results are displayed in Fig. 9. As we can see, such distorted images common in daily life are well rectified by our method.

Besides, as shown in Fig. 10, we also present some handwriting paper cases. It is evident that our method produces neat rectified images with straight textlines, demonstrating its strong generalization ability and robustness.

VI. LIMITATION DISCUSSION

For document image rectification, it is advantageous to extract the cues from the distorted document boundaries and curved textlines that contain the structural information about the page deformation. In particular, for the images without complete document boundaries, it is helpful to exploit the curved textlines in the distorted image that are straight in the rectified one. In this work, our method implicitly encodes such representations, without explicitly considering the geometrical constraints that bridge the distorted and the rectified document images. In future work, we will further explore the potential of these attributes for improving the quality and accuracy of rectified document images.

VII. CONCLUSION

In this study, we introduce DocTr++, a novel deep network for document image rectification. Our method breaks through the scenario limitations of existing rectification methods and is capable of restoring various distorted document images commonly encountered in everyday life. To achieve superior rectification results, we enhance the original DocTr with a hierarchical structure consisting of a distortion encoder and decoder. Additionally, we contribute a real-world test set and new evaluation metrics to assess the quality of rectification for diverse, real-world document images. Through extensive experimentation on both the benchmark dataset and our own proposed dataset, our results demonstrate the efficacy and

superiority of our approach. We hope that our method can serve as a strong baseline for the community, encouraging the further research and development of practical document rectification algorithms.

REFERENCES

- [1] G. Ciardiello, G. Scafuro, M. Degrandi, M. Spada, and M. Roccotelli, “An experimental system for office document handling and text recognition,” in *Proceedings of the International Conference on Pattern Recognition*, 1988, pp. 739–743. [1](#)
- [2] K. Wang, B. Babenko, and S. Belongie, “End-to-end scene text recognition,” in *Proceedings of the International Conference on Computer Vision*, 2011, pp. 1457–1464. [1](#)
- [3] A. Lat and C. Jawahar, “Enhancing OCR accuracy with super resolution,” in *Proceedings of the International Conference on Pattern Recognition*, 2018, pp. 3162–3167. [1](#)
- [4] D. Peng, L. Jin, W. Ma, C. Xie, H. Zhang, S. Zhu, and J. Li, “Recognition of handwritten chinese text by segmentation: a segment-annotation-free approach,” *IEEE Transactions on Multimedia*, 2022. [1](#)
- [5] H. Yuan, Y. Chen, X. Hu, and S. Ji, “Interpreting deep models for text analysis via optimization and regularization methods,” in *Proceedings of the AAAI Conference on Artificial Intelligence*, vol. 33, no. 01, 2019, pp. 5717–5724. [1](#)
- [6] Z. Zhang, J. Ma, J. Du, L. Wang, and J. Zhang, “Multimodal pre-training based on graph attention network for document understanding,” *IEEE Transactions on Multimedia*, 2022. [1](#)
- [7] G. Kim, T. Hong, M. Yim, J. Nam, J. Park, J. Yim, W. Hwang, S. Yun, D. Han, and S. Park, “OCR-free document understanding transformer,” in *Proceedings of the European Conference on Computer Vision*, 2022, pp. 498–517. [1](#)
- [8] G. Salton, “Developments in automatic text retrieval,” *Science*, vol. 253, no. 5023, pp. 974–980, 1991. [1](#)
- [9] Y. Yang, Y.-T. Zhuang, F. Wu, and Y.-H. Pan, “Harmonizing hierarchical manifolds for multimedia document semantics understanding and cross-media retrieval,” *IEEE Transactions on Multimedia*, vol. 10, no. 3, pp. 437–446, 2008. [1](#)
- [10] L. Liu, Y. Lu, and C. Y. Suen, “End-to-end learning of representations for instance-level document image retrieval,” *Applied Soft Computing*, p. 110136, 2023. [1](#)
- [11] M. Mathew, D. Karatzas, and C. Jawahar, “DocVQA: A dataset for VQA on document images,” in *Proceedings of the IEEE Winter Conference on Applications of Computer Vision*, 2021, pp. 2200–2209. [1](#)
- [12] L. Nie, M. Wang, Y. Gao, Z.-J. Zha, and T.-S. Chua, “Beyond text QA: multimedia answer generation by harvesting web information,” *IEEE Transactions on Multimedia*, vol. 15, no. 2, pp. 426–441, 2012. [1](#)
- [13] M. S. Brown and W. B. Seales, “Image restoration of arbitrarily warped documents,” *IEEE Transactions on Pattern Analysis and Machine Intelligence*, vol. 26, no. 10, pp. 1295–1306, 2004. [1, 2](#)
- [14] M. S. Brown and W. B. Seal, “Document restoration using 3D shape,” in *Proceedings of the IEEE International Conference on Computer Vision*, 2001, pp. 9–12. [1, 2](#)
- [15] G. Meng, Y. Wang, S. Qu, S. Xiang, and C. Pan, “Active flattening of curved document images via two structured beams,” in *Proceedings of the IEEE International Conference on Computer Vision*, 2014, pp. 3890–3897. [1, 2](#)
- [16] L. Zhang, Y. Zhang, and C. Tan, “An improved physically-based method for geometric restoration of distorted document images,” *IEEE Transactions on Pattern Analysis and Machine Intelligence*, vol. 30, no. 4, pp. 728–734, 2008. [1, 2](#)
- [17] H. I. Koo, J. Kim, and N. I. Cho, “Composition of a dewarped and enhanced document image from two view images,” *IEEE Transactions on Image Processing*, vol. 18, no. 7, pp. 1551–1562, 2009. [1, 2](#)
- [18] A. Yamashita, A. Kawarago, T. Kaneko, and K. T. Miura, “Shape reconstruction and image restoration for non-flat surfaces of documents with a stereo vision system,” in *Proceedings of the International Conference on Pattern Recognition*, vol. 1, 2004, pp. 482–485. [1](#)
- [19] Y.-C. Tsui and M. S. Brown, “Multi-view document rectification using boundary,” in *Proceedings of the IEEE Conference on Computer Vision and Pattern Recognition*, 2007, pp. 1–8. [1, 2](#)
- [20] Y. Tsui and M. S. Brown, “Geometric and shading correction for images of printed materials: a unified approach using boundary,” in *Proceedings of the IEEE Conference on Computer Vision and Pattern Recognition*, vol. 1, 2004, pp. I–I. [1, 2](#)

[21] S. You, Y. Matsushita, S. Sinha, Y. Bou, and K. Ikeuchi, "Multiview rectification of folded documents," *IEEE Transactions on Pattern Analysis and Machine Intelligence*, vol. 40, no. 2, pp. 505–511, 2018. [1](#), [2](#), [5](#)

[22] C. L. Tan, L. Zhang, Z. Zhang, and T. Xia, "Restoring warped document images through 3D shape modeling," *IEEE Transactions on Pattern Analysis and Machine Intelligence*, vol. 28, no. 2, pp. 195–208, 2006. [1](#), [2](#)

[23] T. Wada, H. Ukida, and T. Matsuyama, "Shape from shading with interreflections under a proximal light source: Distortion-free copying of an unfolded book," *International Journal of Computer Vision*, vol. 24, no. 2, pp. 125–135, 1997. [1](#), [2](#)

[24] Y. He, P. Pan, S. Xie, J. Sun, and S. Naoi, "A book dewarping system by boundary-based 3D surface reconstruction," in *Proceedings of the International Conference on Document Analysis and Recognition*, 2013, pp. 403–407. [1](#), [2](#)

[25] H. Cao, X. Ding, and C. Liu, "Rectifying the bound document image captured by the camera: A model based approach," in *Proceedings of the International Conference on Document Analysis and Recognition*, vol. 1, 2003, pp. 71–75. [1](#), [2](#)

[26] O. Lavialle, X. Molines, F. Angella, and P. Baylou, "Active contours network to straighten distorted text lines," in *Proceedings of the International Conference on Image Processing*, vol. 3, 2001, pp. 748–751. [1](#), [2](#)

[27] C. Wu and G. Agam, "Document image de-warping for text/graphics recognition," in *Proceedings of the Joint IAPR International Workshops on Statistical Techniques in Pattern Recognition and Structural and Syntactic Pattern Recognition*, 2002, pp. 348–357. [1](#), [2](#)

[28] G. Meng, C. Pan, S. Xiang, J. Duan, and N. Zheng, "Metric rectification of curved document images," *IEEE Transactions on Pattern Analysis and Machine Intelligence*, vol. 34, no. 4, pp. 707–722, 2011. [1](#), [2](#)

[29] D. Luo and P. Bo, "Geometric rectification of creased document images based on isometric mapping," *arXiv preprint arXiv:2212.08365*, 2022. [1](#), [2](#)

[30] J. Liang, D. DeMenthon, and D. Doermann, "Geometric rectification of camera-captured document images," *IEEE Transactions on Pattern Analysis and Machine Intelligence*, vol. 30, no. 4, pp. 591–605, 2008. [1](#), [2](#)

[31] M. Liao, Z. Wan, C. Yao, K. Chen, and X. Bai, "Real-time scene text detection with differentiable binarization," in *Proceedings of the AAAI Conference on Artificial Intelligence*, 2020. [1](#)

[32] "Cnstd," <https://github.com/breezedeus/cnstd>, 2023. [1](#)

[33] S. Das, H. M. Sial, R. Baldrich, M. Vanrell, and D. Samaras, "Intrinsic decomposition of document images in-the-wild," in *Proceedings of the British Machine Vision Conference*, 2020. [1](#), [2](#)

[34] S. Das, K. Ma, Z. Shu, D. Samaras, and R. Shilkrot, "DewarpNet: Single-image document unwarping with stacked 3D and 2D regression networks," in *Proceedings of the International Conference on Computer Vision*, 2019, pp. 131–140. [1](#), [2](#), [3](#), [5](#), [6](#), [7](#)

[35] S. Das, K. Y. Singh, J. Wu, E. Bas, V. Mahadevan, R. Bhotika, and D. Samaras, "End-to-end piece-wise unwarping of document images," in *Proceedings of the IEEE International Conference on Computer Vision*, 2021, pp. 4268–4277. [1](#), [2](#), [3](#), [6](#), [7](#)

[36] H. Feng, Y. Wang, W. Zhou, J. Deng, and H. Li, "DocTr: Document image transformer for geometric unwarping and illumination correction," in *Proceedings of the ACM International Conference on Multimedia*, 2021, pp. 273–281. [1](#), [2](#), [3](#), [4](#), [6](#), [7](#), [8](#), [9](#), [10](#)

[37] X. Jiang, R. Long, N. Xue, Z. Yang, C. Yao, and G.-S. Xia, "Revisiting document image dewarping by grid regularization," in *Proceedings of the IEEE Conference on Computer Vision and Pattern Recognition*, 2022, pp. 4543–4552. [1](#), [2](#), [3](#), [6](#), [7](#), [8](#)

[38] X. Liu, G. Meng, B. Fan, S. Xiang, and C. Pan, "Geometric rectification of document images using adversarial gated unwarping network," *Pattern Recognition*, vol. 108, p. 107576, 2020. [1](#), [2](#), [3](#), [7](#)

[39] K. Ma, Z. Shu, X. Bai, J. Wang, and D. Samaras, "DocUNet: Document image unwarping via a stacked U-Net," in *Proceedings of the IEEE International Conference on Computer Vision*, 2018, pp. 4700–4709. [1](#), [2](#), [3](#), [5](#), [6](#), [7](#), [8](#), [9](#), [10](#)

[40] G.-W. Xie, F. Yin, X.-Y. Zhang, and C.-L. Liu, "Document dewarping with control points," in *Proceedings of the International Conference on Document Analysis and Recognition*, 2021, pp. 466–480. [1](#), [2](#), [3](#), [6](#), [7](#)

[41] G. Xie, F. Yin, X. Zhang, and C. Liu, "Dewarping document image by displacement flow estimation with fully convolutional network," in *International Workshop on Document Analysis Systems*. Springer, 2020, pp. 131–144. [1](#), [2](#), [3](#), [6](#), [7](#), [8](#)

[42] C. Xue, Z. Tian, F. Zhan, S. Lu, and S. Bai, "Fourier document restoration for robust document dewarping and recognition," in *Proceedings of the IEEE Conference on Computer Vision and Pattern Recognition*, 2022, pp. 4573–4582. [1](#), [2](#), [3](#), [7](#)

[43] H. Feng, W. Zhou, J. Deng, Q. Tian, and H. Li, "DocScanner: Robust document image rectification with progressive learning," *arXiv preprint arXiv:2110.14968*, 2021. [1](#), [2](#), [3](#), [7](#), [8](#)

[44] H. Feng, W. Zhou, J. Deng, Y. Wang, and H. Li, "Geometric representation learning for document image rectification," in *Proceedings of the European Conference on Computer Vision*, 2022. [1](#), [2](#), [3](#), [6](#), [7](#), [8](#)

[45] A. Markovitz, I. Lavi, O. Perel, S. Mazor, and R. Litman, "Can you read me now? Content aware rectification using angle supervision," in *Proceedings of the European Conference on Computer Vision*, 2020, pp. 208–223. [1](#), [2](#), [3](#), [7](#)

[46] K. Ma, S. Das, Z. Shu, and D. Samaras, "Learning from documents in the wild to improve document unwarping," in *Proceedings of the ACM SIGGRAPH Conference*, 2022, pp. 1–9. [1](#), [2](#), [3](#), [7](#)

[47] J. Zhang, C. Luo, L. Jin, F. Guo, and K. Ding, "Marior: Margin removal and iterative content rectification for document dewarping in the wild," in *Proceedings of the ACM International Conference on Multimedia*, 2022, pp. 2805–2815. [1](#), [2](#), [3](#), [6](#), [7](#), [8](#)

[48] X. Li, B. Zhang, J. Liao, and P. V. Sander, "Document rectification and illumination correction using a patch-based CNN," *ACM Transactions on Graphics*, vol. 38, no. 6, pp. 1–11, 2019. [1](#), [2](#), [3](#), [6](#), [7](#)

[49] Z. Teed and J. Deng, "RAFT: Recurrent all-pairs field transforms for optical flow," in *Proceedings of the European Conference on Computer Vision*, 2020, pp. 402–419. [2](#)

[50] D. Freedman and T. Zhang, "Interactive graph cut based segmentation with shape priors," in *Proceedings of the IEEE Computer Society Conference on Computer Vision and Pattern Recognition*, vol. 1, 2005, pp. 755–762. [2](#)

[51] D. G. Lowe, "Distinctive image features from scale-invariant keypoints," *International Journal of Computer Vision*, vol. 60, no. 2, pp. 91–110, 2004. [2](#)

[52] G. Meng, Y. Su, Y. Wu, S. Xiang, and C. Pan, "Exploiting vector fields for geometric rectification of distorted document images," in *Proceedings of the European Conference on Computer Vision*, 2018, pp. 172–187. [2](#)

[53] O. Ronneberger, P. Fischer, and T. Brox, "U-Net: Convolutional networks for biomedical image segmentation," in *Proceedings of the International Conference on Medical Image Computing and Computer-assisted Intervention*, 2015, pp. 234–241. [3](#)

[54] J. Long, E. Shelhamer, and T. Darrell, "Fully convolutional networks for semantic segmentation," in *Proceedings of the IEEE Conference on Computer Vision and Pattern Recognition*, 2015, pp. 3431–3440. [3](#)

[55] A. Vaswani, N. Shazeer, N. Parmar, J. Uszkoreit, L. Jones, A. N. Gomez, L. Kaiser, and I. Polosukhin, "Attention is all you need," in *Proceedings of the Neural Information Processing Systems*, 2017, pp. 6000–6010. [3](#), [4](#), [9](#)

[56] E. Meijering, "A chronology of interpolation: From ancient astronomy to modern signal and image processing," *Proceedings of the IEEE*, vol. 90, no. 3, pp. 319–342, 2002. [3](#)

[57] F. Verhoeven, T. Magne, and O. Sorkine-Hornung, "Neural document unwarping using coupled grids," *arXiv preprint arXiv:2302.02887*, 2023. [3](#)

[58] K. He, X. Zhang, S. Ren, and J. Sun, "Deep residual learning for image recognition," in *Proceedings of the IEEE Conference on Computer Vision and Pattern Recognition*, 2016, pp. 770–778. [3](#)

[59] I. Bello, B. Zoph, A. Vaswani, J. Shlens, and Q. V. Le, "Attention augmented convolutional networks," in *Proceedings of the IEEE International Conference on Computer Vision*, 2019, pp. 3286–3295. [4](#)

[60] Z. Wang, A. C. Bovik, H. R. Sheikh, and E. P. Simoncelli, "Image quality assessment: from error visibility to structural similarity," *IEEE Transactions on Image Processing*, vol. 13, no. 4, pp. 600–612, 2004. [5](#)

[61] Z. Wang, E. P. Simoncelli, and A. C. Bovik, "Multiscale structural similarity for image quality assessment," in *Proceedings of the Asilomar Conference on Signals, Systems Computers*, vol. 2, 2003, pp. 1398–1402. [5](#)

[62] C. Liu, J. Yuen, and A. Torralba, "SIFT flow: Dense correspondence across scenes and its applications," *IEEE Transactions on Pattern Analysis and Machine Intelligence*, vol. 33, no. 5, pp. 978–994, 2011. [5](#)

[63] V. I. Levenshtein, "Binary codes capable of correcting deletions, insertions, and reversals," vol. 10, pp. 707–710, 1966. [6](#)

[64] I. Loshchilov and F. Hutter, "Decoupled weight decay regularization," in *Proceedings of the International Conference on Learning Representations*, 2019. [6](#)

- [65] L. N. Smith and N. Topin, "Super-convergence: Very fast training of neural networks using large learning rates," in *Artificial Intelligence and Machine Learning for Multi-Domain Operations Applications*, vol. 11006, 2019, p. 1100612. [6](#)
- [66] R. Smith, "An overview of the tesseract OCR engine," in *Proceedings of the International Conference on Document Analysis and Recognition*, vol. 2, 2007, pp. 629–633. [7](#)
- [67] X. Qin, Z. Zhang, C. Huang, M. Dehghan, O. R. Zaiane, and M. Jagersand, "U2-Net: Going deeper with nested U-structure for salient object detection," *Pattern Recognition*, 2020. [8](#)
- [68] N. Carion, F. Massa, G. Synnaeve, N. Usunier, A. Kirillov, and S. Zagoruyko, "End-to-end object detection with transformers," in *Proceedings of the European Conference on Computer Vision*, 2020, pp. 213–229. [10](#)